AIAA JOURNAL
Vol. 30, No. 5, May 1992

Three-Dimensional Strip-Integral Method for Incompressible Turbulent Boundary Layers

Jean Caillé* and Joseph A. Schetz†
Virginia Polytechnic Institute and State University, Blacksburg, Virginia 24061

A three-dimensional, strip-integral method was developed to calculate incompressible turbulent boundary layers. The entrainment coefficient is not required and no empirical relation is needed for the skin-friction coefficient. The Boussinesq assumption is used for the Reynolds stresses, and the eddy viscosity is defined using an extended Clauser outer region model. A practical four-parameter velocity profile was formulated: the streamwise velocity is represented by a new law of the wake based on the Johnston law of the wall and the Moses wake function. The crosswise velocity is represented by the Johnston triangular model. The slope constant is not defined empirically but is directly related to the location of maximum crosswise velocity. Using the momentum integral equations in the streamwise and crosswise directions and two strips gives four equations to solve for four parameters: boundary-layer thickness, skin-friction coefficient, wall crossflow angle, and location of maximum crosswise velocity. The equations are written in nonorthogonal streamline coordinates and are solved using a Runge-Kutta scheme. A comparison with the experimental measurements and other numerical results was achieved for the well-known Van den Berg-Elsenaar and Müller-Krause experiments. Good agreement was generally obtained, and new results are presented for some features of the flow.

Nomenclature

A = normalized wall shear stress
B = constant in wake function
C_f = skin-friction coefficient
C_l = constant in law of the wall
C_{mc} = slope constant in crosswise velocity profile
C_{zx} = eddy viscosity ratio
H = upper limit of control volume
h_x, h_z = metrics
Re_δ = Reynolds number based on boundary-layer thickness
U, W = orthogonal velocity components
$\bar{U}$, $\bar{W}$ = nonorthogonal velocity components
U_e = edge velocity
u, w = Cartesian velocity components
X, Z = nonorthogonal streamline coordinates
x, y, x = Cartesian coordinates
β_w = wall crossflow angle
δ = boundary-layer thickness
δ_1 = streamwise displacement thickness
η = nondimensionalized normal coordinate
λ = nonorthogonal angle
μ_{T_x} = streamwise eddy viscosity
μ_{T_z} = crosswise eddy viscosity
ν = kinematic viscosity
ρ = density
τ = shear stresses

Subscripts

H = upper limit of inner strip
mc = maximum crosswise velocity location
w = wall

Presented as Paper 90-1579 at the AIAA 21st Fluid Dynamics, Plasma Dynamics, and Lasers Conference, Seattle, WA, June 18-20, 1990; received June 28, 1990; revision received Oct. 1, 1990; accepted for publication Oct. 2, 1990.

*Graduate Assistant, Aerospace and Ocean Engineering Department. Student Member AIAA.

†W. Martin Johnson Professor and Head, Aerospace and Ocean Engineering Department. Fellow AIAA.

Introduction

CALCULATION of three-dimensional turbulent flows is essential for today's engineers, and the solution of the governing equations can be obtained using differential or integral methods. The differential methods solve the flow in a domain with three dimensions, and a large number of nodes is required to adequately model the high-velocity gradients in the viscous layer. Because of the fine discretization, the amount of storage is large, and the calculation time becomes impractical for parametric calculations. The integral methods integrate the equations in the direction normal to the wall and solve for practical quantities. One of the best examples is the strip-integral scheme applied to two-dimensional turbulent boundary layers by Moses.[1] As seen in Ref. 2, the Moses two-dimensional strip-integral method performed about as well as the best two-dimensional differential methods on a selection of flows with moderate to high adverse pressure gradients.

The integral methods depend primarily on the parameterization of the velocity profiles; the parameters usually are the boundary-layer thickness, the skin-friction coefficient, and the wall crossflow angle. Two equations are obtained from the conservation of momentum, but with three unknowns and two equations, an additional equation is required. The usual way has been to use an empirical relation for the skin-friction coefficient.[3-9] Furthermore, most prior integral methods make use of the entrainment equation, and more empiricism must be included to define the entrainment coefficient (Refs. 3-9). Therefore, the turbulence modeling tends to be "hidden in opaque correlations."[9] The advantages of the strip-integral method are that an entrainment coefficient is not required, and no empirical relation is needed for the skin-friction coefficient. The turbulence modeling is completely "open" as for differential methods such as Refs. 10 and 11. The number of strips depends on the number of parameters and on the number of equations available per strip. For the two-dimensional formulation, two strips were chosen, because one integral equation is obtained from the conservation of mass and momentum, and the law of the wake is a two-parameter velocity profile.[1] The extension to three-dimensional problems follows the same principle. The conservation of mass and momentum gives two integral equations per strip. It was already mentioned that three-dimensional velocity profiles naturally depend on three parameters. Therefore, at least two strips

should be used, and the problem is now to find additional "natural" parameters.

Based on the conclusions of the excellent review of three-dimensional laws of the wall by Olcmen and Simpson,[12] it was decided to use a new law of the wake based on the Johnston law of the wall[13] with the Moses wake function[1] in the streamwise direction and the Johnston triangular model (see polar plot, Fig. 1) for the crosswise velocity. The streamwise velocity depends on the three usual parameters, whereas the crosswise velocity depends on the streamwise velocity, the wall crossflow angle, and a factor defining the slope of the straight line in region II of the polar plot. This factor is constant across the boundary layer, and can be related to the maximum crosswise velocity and the streamwise velocity at this location. Thus, the location of maximum crosswise velocity is a suitable choice for the fourth parameter. The velocity profile forms a practical four-parameter family, the four parameters being the boundary-layer thickness, the skin-friction coefficient, the wall crossflow angle, and the location of maximum crosswise velocity. Therefore, two strips are used to obtain four equations to solve for the four unknowns.

The integral equations are obtained by applying the principles of conservation of mass and momentum to a three-dimensional control volume of finite height H and infinitesimal base ($dx \times dz$). In Cartesian coordinates, the equations are

$$\frac{\partial}{\partial x}\int_0^H u^2\,dy + \frac{\partial}{\partial z}\int_0^H uw\,dy - u_H\left[\frac{\partial}{\partial x}\int_0^H u\,dy + \frac{\partial}{\partial z}\int_0^H w\,dy\right] = \frac{-H}{\rho}\frac{\partial p}{\partial x} + \frac{(\tau_{xH} - \tau_{xw})}{\rho} \tag{1a}$$

$$\frac{\partial}{\partial z}\int_0^H w^2\,dy + \frac{\partial}{\partial x}\int_0^H uw\,dy - w_H\left[\frac{\partial}{\partial x}\int_0^H u\,dy + \frac{\partial}{\partial z}\int_0^H w\,dy\right] = \frac{-H}{\rho}\frac{\partial p}{\partial z} + \frac{(\tau_{zH} - \tau_{zw})}{\rho} \tag{1b}$$

Based on the experience of other researchers, it was decided to use a nonorthogonal streamline coordinate system. One axis is set along the external streamlines, whereas the direction of the other axis depends on the geometry and the flow conditions. The metrics (h_x and h_z) and the angle between the nonorthogonal axes (λ) are computed numerically at the preprocessing step. The use of nonorthogonal coordinates and the numerical calculation of the metrics insures complete freedom in the creation of the computational domain. Thus, the equations become

$$\frac{1}{q}\frac{\partial}{\partial X}\left(\frac{q}{h_x}\int_0^H \bar{U}^2\,dy\right) + \frac{1}{q}\frac{\partial}{\partial Z}\left(\frac{q}{h_z}\int_0^H \bar{U}\bar{W}\,dy\right) - \frac{\bar{U}_H}{q}\left[\frac{\partial}{\partial x}\left(\frac{q}{h_x}\int_0^H \bar{U}\,dy\right) + \frac{\partial}{\partial z}\left(\frac{q}{h_z}\int_0^H \bar{W}\,dy\right)\right] + K_1\int_0^H \bar{U}^2\,dy + K_2\int_0^H \bar{W}^2\,dy + K_3\int_0^H \bar{U}\bar{W}\,dy = \frac{(\bar{\tau}_{XH} - \bar{\tau}_{XW})}{\rho} + \frac{H\,U_e}{h_x}\left(\frac{\partial U_e}{\partial X} + h_x K_1 U_e\right) \tag{2a}$$

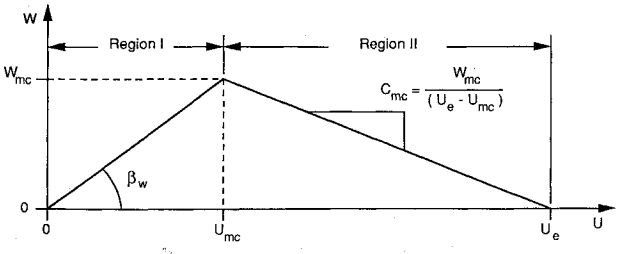

Fig. 1 Johnston triangular model on polar plot.

$$\frac{1}{q}\frac{\partial}{\partial Z}\left(\frac{q}{h_z}\int_0^H \bar{W}^2\,dy\right) + \frac{1}{q}\frac{\partial}{\partial X}\left(\frac{q}{h_X}\int_0^H \bar{U}\bar{W}\,dy\right) - \frac{\bar{W}_H}{q}\left[\frac{\partial}{\partial x}\left(\frac{q}{h_x}\int_0^H \bar{U}\,dy\right) + \frac{\partial}{\partial z}\left(\frac{q}{h_z}\int_0^H \bar{W}\,dy\right)\right] + L_1\int_0^H \bar{U}^2\,dy + L_2\int_0^H \bar{W}^2\,dy + L_3\int_0^H \bar{U}\bar{W}\,dy = \frac{(\bar{\tau}_{ZH} - \bar{\tau}_{ZW})}{\rho} + HU_e^2 L_1 \tag{2b}$$

with

$$q = h_x h_z \sin\lambda$$

$$K_1 = -L_1\cos\lambda$$

$$K_2 = \frac{1}{q\sin\lambda}\left[\frac{\partial(h_x\cos\lambda)}{\partial Z} - \frac{\partial h_z}{\partial X}\right]$$

$$K_3 = \frac{1}{q\sin\lambda}\left[(1+\cos^2\lambda)\frac{\partial h_x}{\partial Z} - 2\cos\lambda\frac{\partial h_z}{\partial Z}\right]$$

$$L_1 = \frac{1}{q\sin\lambda}\left[\frac{\partial(h_z\cos\lambda)}{\partial X} - \frac{\partial h_x}{\partial Z}\right]$$

$$L_2 = -K_2\cos\lambda$$

$$L_3 = \frac{1}{q\sin\lambda}\left[(1+\cos^2\lambda)\frac{\partial h_z}{\partial X} - 2\cos\lambda\frac{\partial h_x}{\partial Z}\right]$$

The pressure gradient was transformed using the equations for the inviscid solution in nonorthogonal coordinates. The inviscid solution, which is used in the integral method through the edge velocity and the description of external streamlines, is from an inviscid calculation or obtained from experimental data when available.

Turbulence Modeling

Contrary to other integral methods, the shear stresses at the top of the inner control volume appear directly in the strip-integral formulation. The Boussinesq assumption relates the shear stresses to the velocity gradients:

$$\bar{\tau}_{XH} = \mu_{T_x}\frac{\partial \bar{U}}{\partial y} \tag{3a}$$

$$\bar{\tau}_{ZH} = \mu_{T_z}\frac{\partial \bar{W}}{\partial y} \tag{3b}$$

with

$$\mu_{T_z} = C_{zx}\mu_{T_x}$$

Here, μ_{T_x} is the streamwise eddy viscosity and μ_{T_z} is the crosswise eddy viscosity. Previous experiments have shown that the ratio of eddy viscosities C_{zx} can be smaller or greater than 1. The influence of C_{zx} was studied for one test case, and the analysis is presented in the section "Results and Discussion." It should be noted that a value of 1.0 would be adequate when no information is available about the flow.

The streamwise eddy viscosity is taken here as defined by the Clauser outer region model. This model has proven adequate for two-dimensional analyses, and the extension to a three-dimensional analysis is straightforward:

$$\mu_{T_x} = 0.0168\rho U_e\delta_1 \tag{4}$$

where δ_1 is the streamwise displacement thickness. A model for the inner region is not required, because the shear stresses

are computed at the upper limit of the inner strip, which is always chosen in the outer region of the boundary layer. This turbulence model is simple and adequate for most three-dimensional analyses, but, if necessary, a more sophisticated model (e.g., TKE, k-ϵ, etc.) can be implemented easily without changing the basic formulation.

Velocity Profiles

The integral methods depend primarily on the parameterization of the velocity profiles. Here a practical four-parameter velocity profile was chosen for reasons mentioned previously. The total velocity is divided into two components. The first component is in the direction of the tangent to the external streamlines, and the second component is perpendicular to the first one. Therefore, the velocity profile is expressed in streamline orthogonal coordinates and must be transformed to the nonorthogonal coordinate system before integration. In the streamwise direction, the law of the wake is constructed from the Johnston law of the wall and the Moses wake function. The crosswise velocity is obtained by the Johnston triangular model (see polar plot, Fig. 1). The orthogonal components of the velocity profile are written as

$$U/U_e = A\cos\beta_w \ln(C_l A Re_\delta \eta) - B\eta^2(3-2\eta) \qquad (5a)$$

and

$$W/U_e = U/U_e \tan\beta_w \qquad \text{for } \eta < \eta_{mc} \qquad (5b)$$

or

$$W/U_e = C_{mc}(1 - U/U_e) \qquad \text{for } \eta > \eta_{mc} \qquad (5c)$$

with

$$A = 1/\kappa\sqrt{C_f/2}$$

$$B = A\cos\beta_w \ln(C_l A Re_\delta) - 1$$

$$C_{mc} = \frac{W_{mc}/U_e}{1 - U_{mc}/U_e}$$

$$\kappa = 0.41$$

$$C_l = 3.057$$

$$Re_\delta = U_e\delta/\nu$$

$$\eta = y/\delta$$

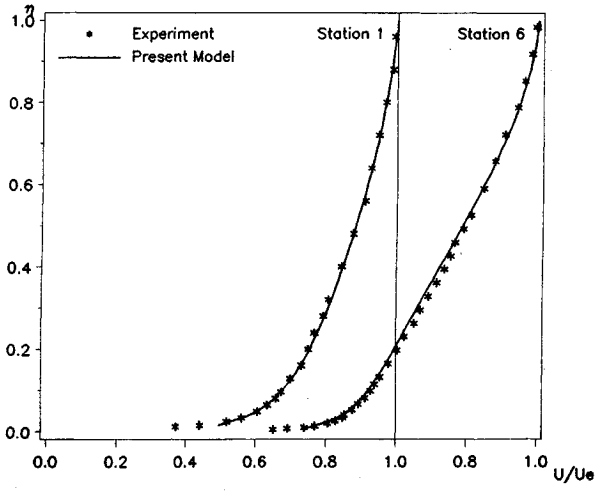

Fig. 2 Comparison of the streamwise velocity profile model with the Van den Berg-Elsenaar measurements at two stations.

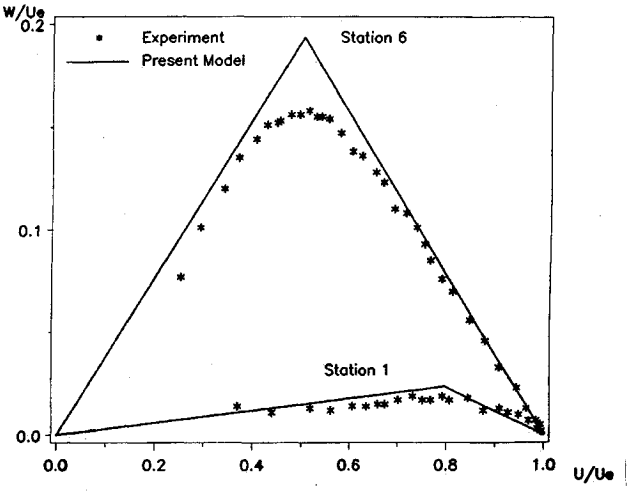

Fig. 3 Comparison of the crosswise velocity profile model with the Van den Berg-Elsenaar measurements at two stations on polar plot.

The location of maximum crosswise velocity is η_{mc}. U_{mc} and W_{mc} are, respectively, the streamwise and crosswise velocity at this location. A comparison was made with the velocity profile at two typical stations from the Van den Berg-Elsenaar experiment. Figures 2 and 3 show excellent agreement.

Differential Equations

Two momentum integral equations were written in nonorthogonal streamline coordinates for an arbitrary control volume, and a velocity profile was formulated with four parameters. Four equations are obtained by using two strips. The first strip is the entire boundary layer. Therefore, the two integral equations for this strip assume the general form used by other integral methods. At the edge of the boundary layer, the velocity becomes the edge velocity, and the shear stresses are zero. The inner strip goes from the wall up to a location inside the boundary layer. The upper limit of the inner strip η_H is arbitrary, but good results are obtained for η_H in the range [0.20,0.40]. The velocities and velocity gradients at that location are obtained from the velocity profile previously defined.

After integration of the velocity profiles and expansion of the streamwise derivatives, the following form is obtained for the set of equations:

$$C_{i1}\frac{\partial A}{\partial X} + C_{i2}\frac{\partial \beta_w}{\partial X} + C_{i3}\frac{\partial Re_\delta}{\partial X} + C_{i4}\frac{\partial \eta_{mc}}{\partial X} = F_i \qquad i = 1,4 \qquad (6)$$

where the right-hand sides contain all derivatives with respect to the crosswise direction. The coefficients and the right-hand sides are functions of the four unknowns, the edge velocity, and the form of the mesh, which is described by the shape of the external streamlines, and the metrics of the transformation to nonorthogonal coordinates.

Numerical Procedure

The previous differential equations are hyperbolic.[8] The characteristics at a point over the surface are all located between the external streamlines and the wall streamlines (also called skin-friction lines). The shape of the characteristics and the orientation of one with respect to the other affect the discretization of the equations and the implementation of the boundary conditions. The numerical domain of dependence must include the physical domain of dependence (CFL condition), and boundary conditions are needed along the sides where the flow comes into the computational domain.

Starting from the initial location where the solution is known along the entire line, the solution is computed over the wall using a space marching technique. The numerical integration is done using a Runge-Kutta scheme.

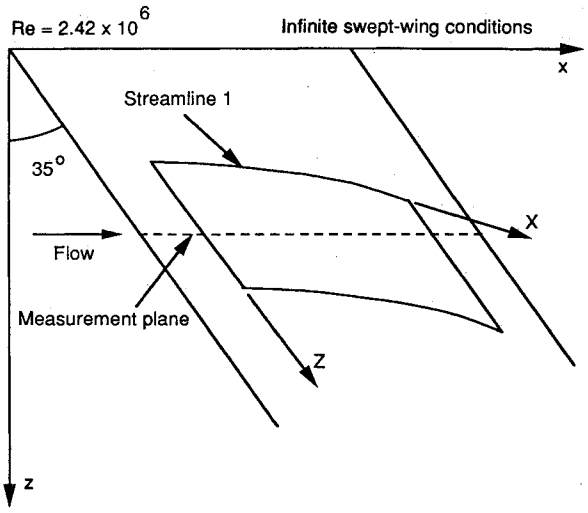

Fig. 4 Van den Berg-Elsenaar flow: computational domain.

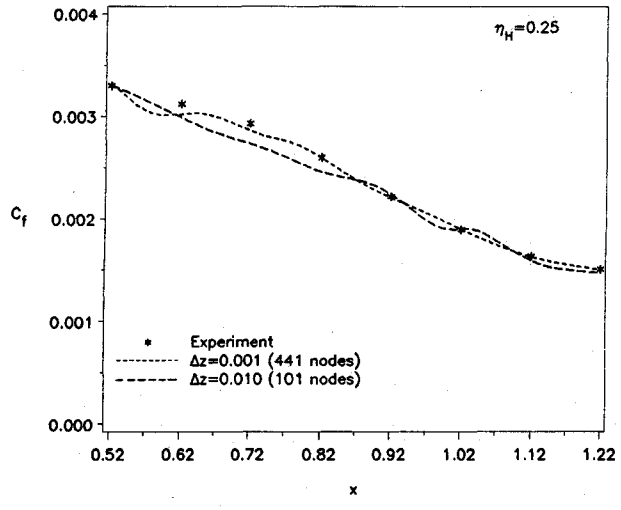

Fig. 5 Van den Berg-Elsenaar flow: comparison for the skin-friction coefficient.

Integral methods do not require a large amount of storage, and the calculation time is very small. On the IBM 3090, the CPU time was less than 5 s for all computations. It would be possible to use much smaller computers (even personal computers) to get accurate solutions in real time with the strip-integral method.

Results and Discussion

Two experiments were used to validate the present strip-integral method. A study of three-dimensional turbulent boundary layers was done for the 1980–81 Stanford Conference,[14] which was followed in 1982 by an EUROVISC workshop.[15] The Van den Berg-Elsenaar and Müller-Krause experiments were chosen as test cases for numerical methods and are, therefore, well known and fully documented. The present numerical results are compared with the experimental measurements and other numerical predictions (obtained from Ref. 15) for the skin-friction coefficient, the wall crossflow angle, the boundary-layer thickness, and the streamwise displacement thickness.

Van den Berg-Elsenaar Flow

The flow over a flat surface with a 35 deg sweep angle under infinite swept-wing conditions in an adverse pressure gradient was investigated by Van den Berg and Elsenaar.[16,17] Information about the computational domain is presented in Fig. 4. The flow characteristics were computed for the first eight stations (following the original numbering convention of the investigators). Separation occurs near station 9, and the present method cannot be applied for separated flow. The width of the computational region is somewhat artificial, because the infinite swept-wing conditions mean that there is no variation in the spanwise direction (parallel to the leading edge).

The solution was computed along a streamline, with $\eta_H = 0.25$. Starting from station 1 and using the "exact" values as boundary conditions along streamline 1, the solution was computed on the adjacent streamline for two different crosswise step sizes: 0.01 and 0.001. The results are shown in Figs. 5 and 6 for the skin-friction coefficient and wall crossflow angle, respectively. For these calculations, the hyperbolic character of the equations becomes important. The streamwise step size must be set depending on the crosswise step size following the CFL condition. As expected, the agreement with the measurements is better for a smaller Δz. Good agreement was globally obtained. Contrary to most previous predictions for this case, the wall crossflow angle does not start to decrease after $x = 1.12$. The general trend is well-represented when approaching separation, even if a simple turbulence model is used for the present method. The results for the

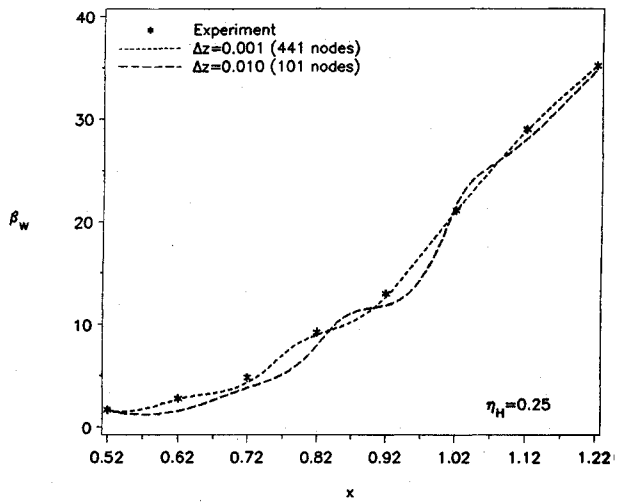

Fig. 6 Van den Berg-Elsenaar flow: comparison for the wall crossflow angle.

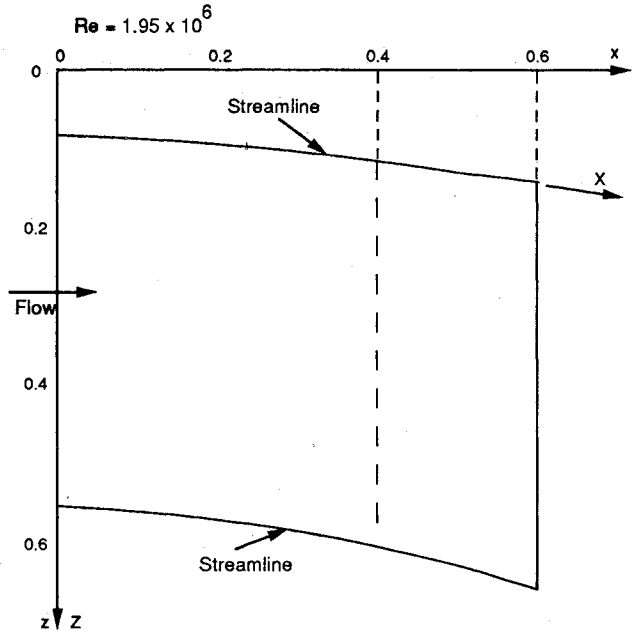

Fig. 7 Müller-Krause flow: computational domain.

wall crossflow angle show a wavy character. This behavior can be explained by the strong dependency of the wall crossflow angle on the location of maximum crosswise velocity (see Fig. 1), which shows some numerical sensitivity.

Müller-Krause Flow

The second case is the flow over a flat surface with an adverse pressure gradient in the streamwise direction and an induced pressure gradient in the crosswise direction. This flow was designed and studied by Müller and Krause.[18] Information concerning the geometry of the computational domain is presented in Fig. 7.

The complete results along a line parallel to the z axis are shown in Figs. 8–11 for $x = 0.4$, and in Figs. 12–15 for $x = 0.6$. The upper limit of the inner strip is located at 0.35, and the eddy viscosity ratio is set to 1.2 following the recommendation of Müller. A relatively coarse mesh was used: 81 nodes in the streamwise direction and 41 nodes in the crosswise direction. A finer mesh (161 × 81) was also used without any improvements. The overall agreement is good. The present predictions are even more impressive, considering the results obtained by the differential methods of Müller and Patel et al.[15] The strip-integral method gives equivalent or better results at a fraction of the cost of a differential method. Again, the results show a wavy character depending on the location of maximum crosswise velocity. The values of η_{mc} used as boundary conditions along the inside streamline were extracted from the measured velocity profiles. These values are approximate, and they have a strong influence on the solution near the inside streamline.

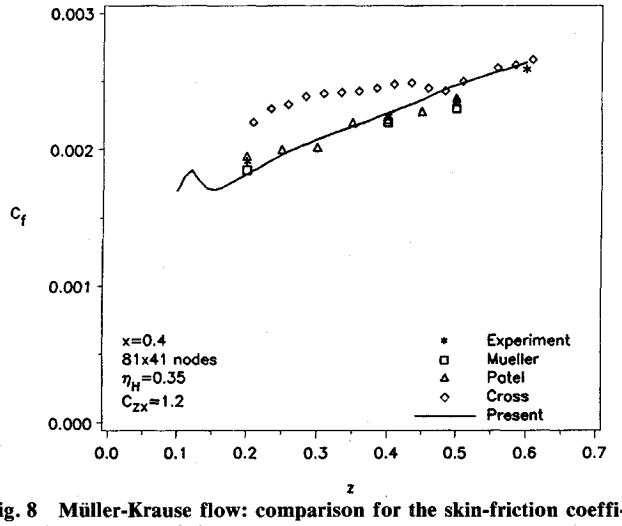

Fig. 8 Müller-Krause flow: comparison for the skin-friction coefficient along z at $x = 0.4$.

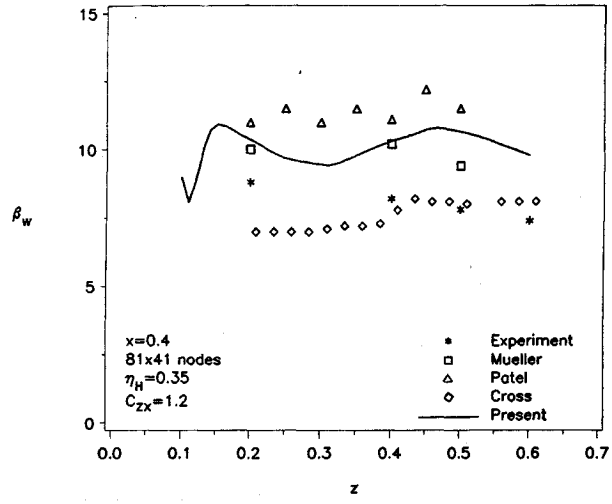

Fig. 9 Müller-Krause flow: comparison for the wall crossflow angle along z at $x = 0.4$.

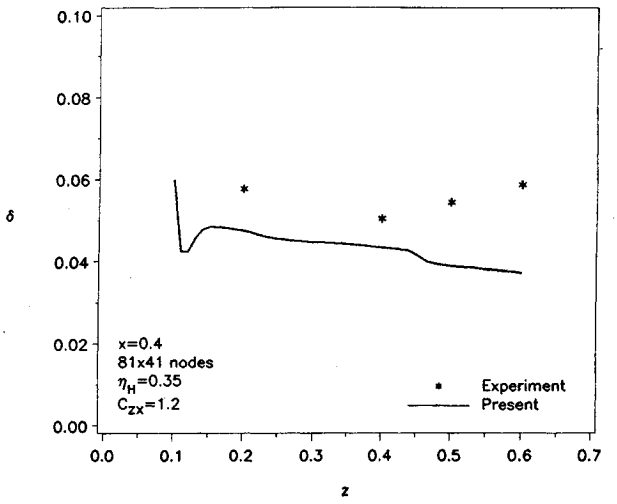

Fig. 10 Müller-Krause flow: comparison for the boundary-layer thickness along z at $x = 0.4$.

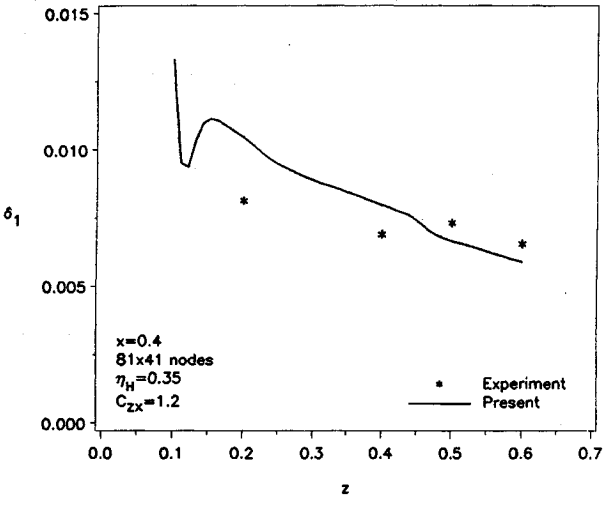

Fig. 11 Müller-Krause flow: comparison for the streamwise displacement thickness along z at $x = 0.4$.

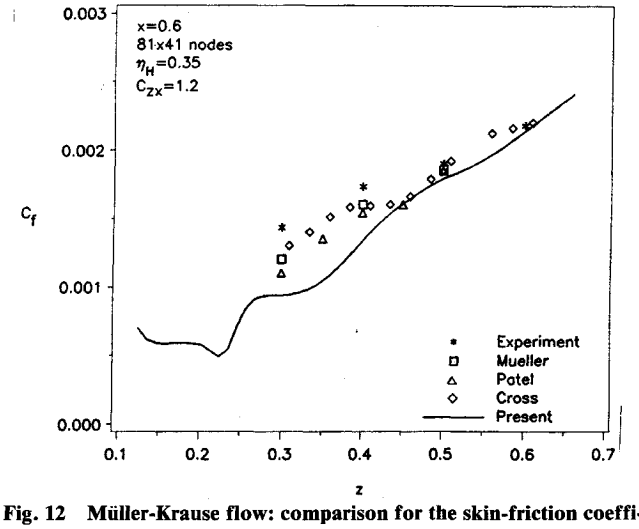

Fig. 12 Müller-Krause flow: comparison for the skin-friction coefficient along z at $x = 0.6$.

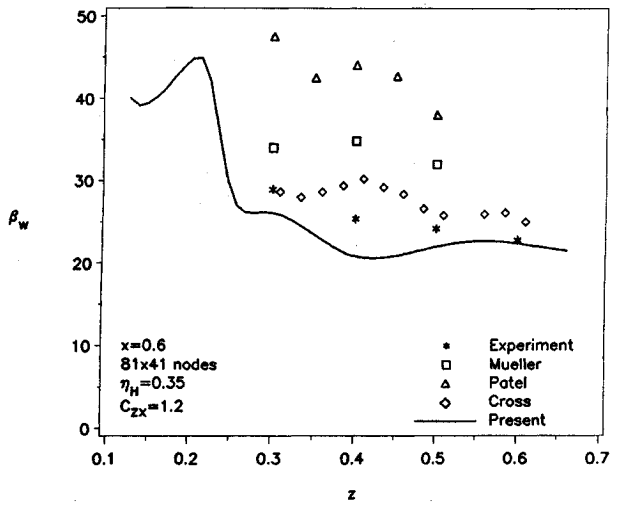

Fig. 13 Müller-Krause flow: comparison for the wall crossflow angle along z at $x = 0.6$.

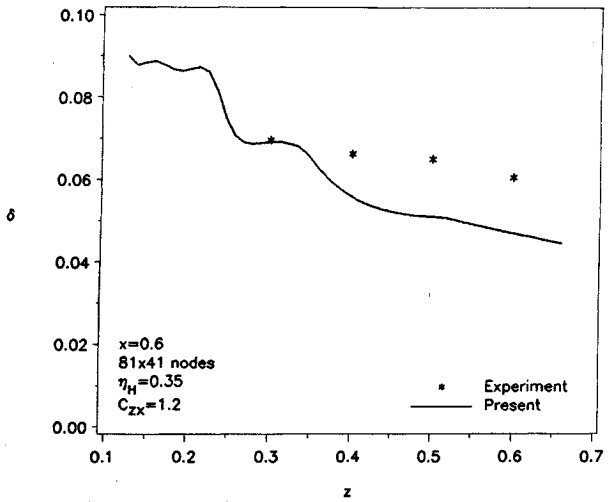

Fig. 14 Müller-Krause flow: comparison for the boundary-layer thickness along z at $x = 0.6$.

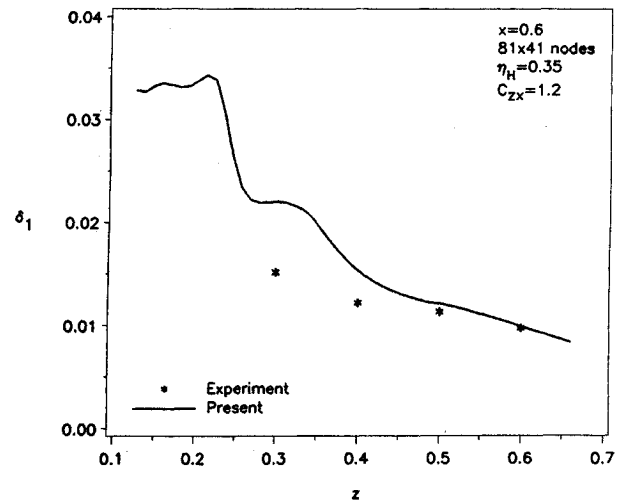

Fig. 15 Müller-Krause flow: comparison for the streamwise displacement thickness along z at $x = 0.6$.

The influence of the inner-strip upper limit on the skin-friction coefficient and the wall crossflow angle was studied, and the results are shown in Figs. 16 and 17 for the line $x = 0.6$. The same node distribution was also used. The influence of η_H is important for the present case; larger values give better overall results. For the earlier case, the results were less sensitive to η_H.

The influence of the eddy viscosity ratio was also studied. The results for the wall crossflow angle are shown in Fig. 18

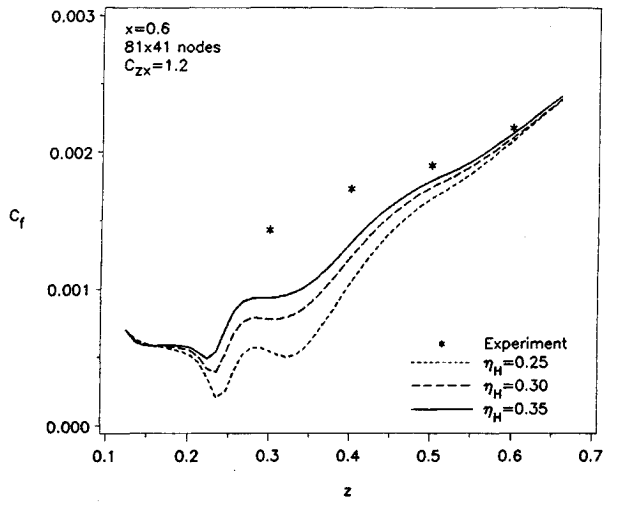

Fig. 16 Müller-Krause flow: influence of the location of the inner strip upper limit on the results for the skin-friction coefficient at $x = 0.6$.

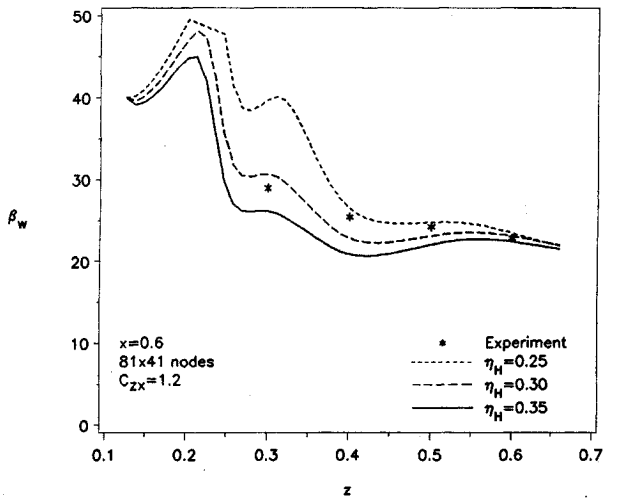

Fig. 17 Müller-Krause flow: influence of the location of the inner strip upper limit on the results for the wall crossflow angle at $x = 0.6$.

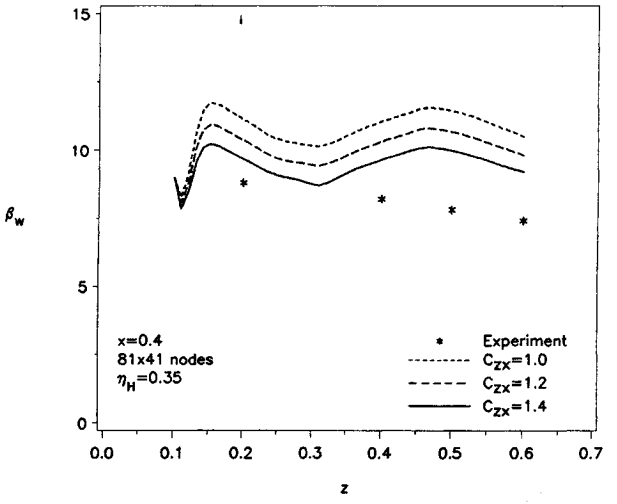

Fig. 18 Müller-Krause flow: influence of the eddy viscosity ratio on the results for the wall crossflow angle at $x = 0.4$.

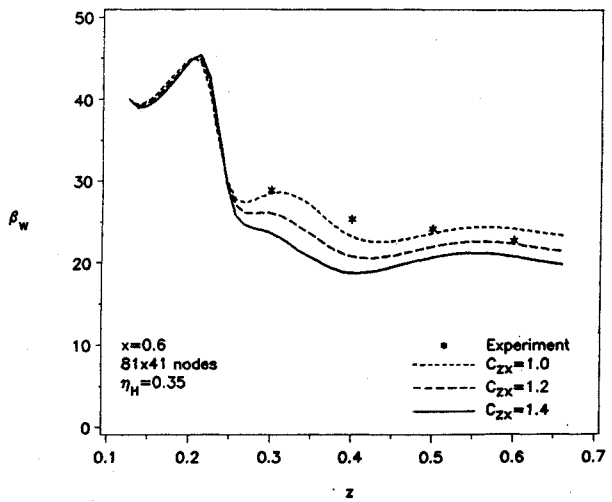

Fig. 19 Müller-Krause flow: influence of the eddy viscosity ratio on the results for the wall crossflow angle at $x = 0.6$.

for $x = 0.4$ and in Fig. 19 for $x = 0.6$. Three values were used: 1.0, 1.2, and 1.4. At $x = 0.4$, a value of 1.4 gives better results, whereas a value of 1.0 is more appropriate at $x = 0.6$. When no information is available about the shear stresses, a value of unity would prove adequate.

Conclusions

A three-dimensional integral method was developed to calculate three-dimensional, incompressible turbulent boundary layers. This new method is based on the strip-integral formulation. The number of strips is chosen according to the number of parameters in the velocity profile. This means that the entrainment equation is not required, and no empirical relation is needed for the skin-friction coefficient. The Boussinesq assumption was used for the Reynolds stresses, and the streamwise eddy viscosity was defined using the Clauser outer region model. This simple model proved adequate for the present applications. The implementation of a more sophisticated model is also possible and can be done without changing the basic formulation.

A practical four-parameter velocity profile was formulated based on the Johnston law of the wall and triangular model. The slope constant was not defined empirically, but was related to the location of maximum crosswise velocity, which is one of the four parameters, along with the skin-friction coefficient, the wall crossflow angle, and the boundary-layer thickness.

The equations were written in nonorthogonal streamline coordinates to assure full flexibility in the construction of the computational domain. Two strips were used to solve for the four unknowns. The upper limit of the inner strip is arbitrary, but optimal results were obtained for values in the range [0.20,0.40]. The set of differential equations was solved using a Runge-Kutta scheme with a space marching technique. All computations were performed in less than 5 s of CPU time on an IBM 3090.

A comparison with the experimental measurements and other numerical results was achieved for the well-known Van den Berg-Elsenaar and Müller-Krause experiments. The location of maximum crosswise velocity has an influence on the behavior of the solution. The eddy viscosity ratio also influences the numerical results, but when no information is available, a value of unity would prove adequate. The present integral analysis provided predictions as good as or better than the competing differential methods at a small fraction of the computational cost.

Acknowledgments

This work was supported mainly by the Office of Naval Research, with James Fein as Technical Monitor, and by the Cornell Theory Center, including the Cornell National Supercomputer Facility.

References

[1]Moses, H. L., "A Strip-Integral Method for Predicting the Behavior of Turbulent Boundary Layers," *Proceedings Computation of Turbulent Boundary Layers—1968 AFOSR-IFP-STANFORD Conference,* Vol. 1, Stanford Univ., Stanford, CA, 1969, pp. 76–82.

[2]Coles, D. E., and Hirst, E. A., *Proceedings Computation of Turbulent Boundary Layers—1968 AFOSR-IFP-STANFORD Conference,* Vol. 2, Stanford Univ., Stanford, CA, 1969.

[3]Smith, P. D., "An Integral Prediction Method for Three-Dimensional Compressible Turbulent Boundary Layers," Royal Aircraft Establishment, TR 72228, England, UK, 1972.

[4]Smith, P. D., "The Numerical Computation of Three-Dimensional Boundary Layers," *Three-Dimensional Boundary Layers,* edited by H. H. Fernholz and E. Krause, Springer-Verlag, Berlin, 1982.

[5]Lazareff, M., and Le Balleur, J. C., "Computation of Three-Dimensional Viscous Flows on Transonic Wings by Boundary Layer-Inviscid Flow Interaction," Recherche Aerospatiale, 1983.

[6]Cross, A. G. T., "Calculation of Compressible Three-Dimensional Turbulent Boundary Layers with Particular Reference to Wings and Bodies," British Aerospace (Brough) Note YAD 3379, 1979.

[7]Cross, A. G. T., "Two-Dimensional Boundary Layer Calculations Using a Three Parameter Velocity Profile," British Aerospace (Brough) Note YAD 3428, 1980.

[8]Cousteix, J., and Michel, R., "Three-Dimensional Turbulent Boundary Layer Calculations," *Perspectives in Turbulence Studies, International Symposium,* Göttingen, Germany, May 11–12, 1987, pp. 439–472.

[9]Humphreys, D. A., and Lindhout, J. P. F., "Calculation Methods for Three-Dimensional Turbulent Boundary Layers," *Progress in Aerospace Sciences,* Vol. 25, 1988, pp. 107–129.

[10]Cebeci, T., "Calculation of Three-Dimensional Boundary Layers II. Three-Dimensional Flows in Cartesian Coordinates, *AIAA Journal,* Vol. 13, No. 8, pp. 1056–1064.

[11]Pierce, F. J., and Klinksiek, W. F., "An Implicit Numerical Solution of the Turbulent Three-Dimensional Incompressible Boundary Layer Equations," Virginia Polytechnic Inst. and State Univ., Blacksburg, VA, VPI-E-71-14, 1971.

[12]Olcmen, S., and Simpson, R. L., "Some Near Wall Features of Three-Dimensional Turbulent Boundary Layers," Fourth Symposium on Numerical and Physical Aspects of Aerodynamic Flows, Long Beach, CA, Jan. 1989.

[13]Johnston, J. P., "On the Three-Dimensional Turbulent Boundary Layer Generated by Secondary Flow," *Journal of Basic Engineering,* Vol. 82, No. 1, March 1960, pp. 233–248.

[14]Kline, S. J., Cantwell, B. J., and Lilley, G. M., *1980-81 AFOSR-HTTM-STANFORD Conference on Complex Turbulent Flows,* Vols. 1–3, Stanford Univ., Stanford, CA, 1981.

[15]Van den Berg, B., Humphreys, D. A., Krause, E., and Lindhout, J. P. F., "Three-Dimensional Turbulent Boundary Layers—Calculations and Experiments," *Notes on Numerical Fluid Mechanics,* Vol. 19, Vieweg, Braunschweig, Germany, 1988, p. 163.

[16]Van den Berg, B., and Elsenaar, A., "Measurements in a Three-Dimensional Incompressible Turbulent Boundary Layer in an Adverse Pressure Gradient Under Infinite Swept Wing Conditions," National Aerospace Lab., TR 72092 U, The Netherlands, 1972.

[17]Van den Berg, B., Elsenaar, A., Lindhout, J. P. F., and Wesseling, P., "Measurements in an Incompressible Three-Dimensional Turbulent Boundary Layer, Under Infinite Swept-Wing Conditions, and Comparison with Theory," *Journal of Fluid Mechanics,* Vol. 70, Pt. 1, 1975, pp. 127–148.

[18]Müller, U. R., "Measurements of the Reynolds Stresses and the Meanflow Field in a Three-Dimensional Pressure-Driven Boundary Layer," *Journal of Fluid Mechanics,* Vol. 119, June 1982, pp. 121–153.